

Synthesis, Characterization, In Vivo Imaging, Hemolysis, and Toxicity of Hydrophilic Ag₂S Near-Infrared Quantum Dots

Jaber Javidi¹ · Azadeh Haeri¹ · Farshad Hosseini Shirazi² · Farzad Kobarfard³ · Simin Dadashzadeh^{1,4}

Received: 12 April 2016 / Published online: 16 August 2016
© Springer Science+Business Media New York 2016

Abstract Ag₂S quantum dots (Qds) are a new type of near-infrared Qds and hold great potential for in vivo imaging. There is great demand for versatile, practical, and environmentally-friendly processes for formation of hydrophilic Ag₂S Qds. The present study prepared hydrophilic Ag₂S near-infrared Qds using a simple, easy, one-step method. The Qds were characterized by TEM, XRD, FT-IR, UV–Visible and PL spectroscopy and the effect of the reaction variables of time, temperature, precipitation agent feeding rate, and S:Ag molar ratio on the size and PL spectrum of the Ag₂S Qds was investigated. The Qds exhibited near-infrared photoluminescence and good photostability, which was evaluated under different conditions. Cytotoxicity tests were carried out on human A549 and Hep G2 cell lines at concentrations of 6.25–200 µg/ml. MTT assay revealed that the Qds showed no significant toxicity. The effect of plasma and corona proteins on the hemolytic activity of Ag₂S Qds in four concentrations was evaluated for rat and human red blood cells. In vivo imaging showed that the Ag₂S Qds penetrated the body of mice with excellent brightness. The hydrophilic Ag₂S Qds can be safely applied as near-infrared optical imaging probes for nanodiagnostics or in vivo imaging.

✉ Simin Dadashzadeh
Sdadashzadeh@sbmu.ac.ir; dadashzadeh5@yahoo.com

¹ Department of Pharmaceutics, School of Pharmacy, Shahid Beheshti University of Medical Sciences, P.O. Box 14155-6153, Tehran, Iran

² Department of Toxicology, School of Pharmacy, Shahid Beheshti University of Medical Sciences, Tehran, Iran

³ Department of Medicinal Chemistry, School of Pharmacy, Shahid Beheshti University of Medical Sciences, Tehran, Iran

⁴ Pharmaceutical Sciences Research Center, Shahid Beheshti University of Medical Sciences, Tehran, Iran

Keywords Silver sulfide · Quantum dots · In vivo imaging · Protein corona · MTT Assay

Introduction

In recent decades, inorganic nanostructures such as super-paramagnetic nanoparticles [1], gold nanoparticles [2], mesoporous silica nanoparticles [3] and quantum dots (Qds) have been developed for use in biomedical applications and cancer nanotechnology [4–7]. Among these nano-platforms, Qds have been intensively investigated for tumor diagnostics or as imaging markers [8], bio-indicators [9], drug delivery systems [10], and therapeutic medicine [11]. Qds are luminescent semi-conducting nanocrystals 2–100 nm in diameter that contain coupled elements such as II B–VI A, III A–V A, and IV A elements [12]. When compared with other common organic dyes, Qds have shown optical advantages, including intense brightness caused by an extinction coefficient and quantum yield, high sensitivity, broad absorption properties, a narrow emission band, and size dependent emission spectra.

Despite these advantages, Qds with luminescence in the visible region (400–700 nm) has not been preferred for use because it is affected by scattering interference of biological materials such as water, hemoglobin, and deoxyhemoglobin, autofluorescence of native tissues in this region, and the low depth of penetration of visible light. Near-infrared (NIR) region I (700–900 nm) and II (1000–1300 nm) are suitable fluorescence imaging windows because they offer minimal body autofluorescence, negligible tissue scattering interference, and maximal penetration depth [13, 14]. The types of NIR Qds reported thus far are CdSeTe [15], CdHgTe/CdS [16], CdTe/CdSe/ZnSe [17], and PbS [18]. Although the fluorescence properties of these Qds are appropriate for in vivo imaging, leakage of toxic elements (Cd, Hg, Pb, Te and Se) is an important limitation to their practical use.

Ag₂S Qds are a new type of NIR Qds that are free of toxic elements and are highly stable ($K_{sp} = 6.3 \times 10^{-50}$). They have been applied by researchers for anatomical imaging [19], tumor diagnosis [20–23], drug delivery [24, 25], and are conjugated with different targeting moieties for tumor targeting [24, 26, 27]. A number of synthesis methods have been reported for Ag₂S Qds [20, 23, 28–32]; however, most suffer from drawbacks such as long reaction time, high temperature, use of harmful organic solvents, and multi-step procedures [33, 34].

A method was developed by Martinez-Castanon et al. [35] for synthesis of Ag₂S utilizing aqueous media, but the resulting particles were larger than 30 nm and no data on optical characteristics was available. Hocaoglu et al. [36] and Jiang et al. [23] prepared hydrophilic Ag₂S Qds under an argon atmosphere. Yang et al. [29] prepared hydrophilic Ag₂S Qds in the presence of bovine serum albumin, but the reaction time was lengthy and the purification method was tedious. There remains great demand for versatile, simple, and environmentally-friendly processes for formation of hydrophilic Ag₂S Qds under simple and practical conditions.

The present study developed an easy, one-step, and simple method for preparation of hydrophilic Ag_2S in aqueous media. The effect of reaction variables such as time, temperature, precipitation agent feeding rate, and S:Ag molar ratio on the size and photoluminescence (PL) of Ag_2S Qds was demonstrated. The photostability of the Qds was examined under various conditions.

Ag_2S Qds was investigated for toxicity and interaction with cells before consideration for bioapplications. To evaluate the biocompatibility of the Qds, hemolysis and cytotoxicity tests were carried out on rat and human RBCs and human A549 and Hep G2 cell lines, respectively. The effect of plasma and corona proteins on the hemolytic activity of Ag_2S Qds at various concentrations was also evaluated. Dawson et al. reported that the adsorption of the plasma component onto the surface of nanoparticles leads to formation of a stable coating called a protein corona [37]. This coating could alter the interaction between nanoparticles and RBCs. To the best of our knowledge, no literature reports on the role of the protein corona in the interaction of Ag_2S Qds with RBCs. The present study also demonstrated the in vivo imaging ability of Ag_2S Qds.

Experimental

Materials and Physical Measurements

Chemical reagents used in the experiments were purchased from Merck Co. (Darmstadt, Germany) and were used without further purification. Fourier transform infrared (FTIR) spectra were obtained using a Shimadzu FT-IR 8300 spectrophotometer. X-ray powder diffraction (XRD) analysis was conducted on a Bruker AXS D8-advance X-ray diffractometer using Cu K_α radiation ($\lambda = 1.5418 \text{ \AA}$). Transmission electron microscopy [38] images were obtained on a Philips EM208 transmission electron microscope with an accelerating voltage of 100 kV.

Preparation of Ag_2S Qds

Hydrophilic Ag_2S Qds were prepared by coprecipitation. In a typical procedure, 0.2 g of AgNO_3 was dissolved in a solution of ethylene glycol and water (20:80 v/v) and the resultant solution was stirred continuously at $100 \text{ }^\circ\text{C}$ and 800 rpm for 0.5 h. Mercaptoacetic acid [39] was then added dropwise under vigorous stirring. After a few minutes, the color of solution changed from yellow to milky and finally to brown. The Qds were cooled to room temperature and then centrifuged at 14,000 rpm for 20 min. The influence of reaction time, temperature, MAA:Ag molar ratio, and feeding rate were investigated. Table 1 shows the conditions of the reactions in detail. The goal of producing Ag_2S Qds was their application as an in vivo imaging marker; therefore, sample 13 was chosen for further characterization because it emitted at a higher wavelength (785 nm) when compared with the other samples.

The particle sizes of Qds was calculated by Brus equation [40] (Eq. 1) as:

Table 1 Experimental conditions for the preparation of Ag₂S Qds (mean ± SD, n = 3)

No.	Time (h)	Tem. (°C)	MAA:Ag molar ratio	F.R ^a (μl/min)	λ _{max}	E _g (eV)	λ _{em}
1	1	RT	4	10	255.7 ± 1.5	4.85 ± 0.03	538.7 ± 1.1
2	1	50	4	10	347.6 ± 1.5	3.57 ± 0.02	547.2 ± 1.2
3	1	100	4	10	350.3 ± 0.6	3.53 ± 0.01	550.3 ± 0.6
4	2	RT	4	10	346.3 ± 1.5	3.58 ± 0.02	646.3 ± 1.5
5	2	50	4	10	350.7 ± 1.2	3.54 ± 0.01	651.6 ± 1.5
6	2	100	4	10	356.3 ± 1.5	3.48 ± 0.01	656.3 ± 1.5
7	3	RT	4	10	357.7 ± 1.5	3.46 ± 0.02	657.3 ± 2.1
8	3	50	4	10	378.7 ± 1.5	3.27 ± 0.01	751.6 ± 2.1
9	3	100	4	10	391.3 ± 1.5	3.16 ± 0.03	784.6 ± 0.6
10	3	100	2	10	280.3 ± 1.5	4.42 ± 0.02	541.7 ± 2.0
11	3	100	2	100	321.3 ± 1.5	3.85 ± 0.02	544.6 ± 1.5
12	3	100	2	1000	366.3 ± 1.1	3.38 ± 0.01	643.3 ± 2.5
13	3	100	4	100	484.7 ± 1.5	2.58 ± 0.01	785.5 ± 2.3
14	3	100	4	1000	570.7 ± 0.6	2.17 ± 0.01	–
15	3	100	6	10	482.7 ± 2.5	2.56 ± 0.01	–
16	3	100	6	100	561.7 ± 1.5	2.21 ± 0.01	–
17	3	100	6	1000	602.3 ± 2.5	2.06 ± 0.01	–

^a Feeding rate

$$E_g = E_{g(b)} + \frac{h^2}{8R^2} \left(\frac{1}{m_e} + \frac{1}{m_h} \right) \quad (1)$$

where E_g and $E_{g(b)}$ are the band gap energy of the nano and bulk nanocrystal, respectively (for bulk Ag₂S, $E_{g(b)} = 0.85$), R is the radius of the nanocrystals, m_e ($0.286 m_0$) and m_h (1.096) are the effective electron and hole masses of the Ag₂S, respectively [41], and h is Planck's constant (4.13×10^{-15} eV). Equation 2 was obtained by substituting the these values in Eq. 1,

$$R = \left(\frac{10.3577}{E_g - 0.85} \right)^{1/2} \quad (2)$$

The band gap energy of the Qds [35] was calculated as:

$$E_g = \frac{1240}{\lambda_{\max}} \text{ (eV)} \quad (3)$$

Stability of Ag₂S Qds

The PL stability of Ag₂S Qds was studied under different conditions. To evaluate the effect of storage temperature on the PL spectra, 0.2 μg/ml of Qds were

incubated with phosphate buffer saline (PBS; 1 mM; pH 7.0) at either ° or 37 °C for 24 h. The PL intensity of the QDs was recorded at different concentrations (0.01, 0.1, and 0.2 µg/ml) and time intervals (immediately, 48 h, and 2 weeks) at 4 °C following storage in either transparent or opaque vials. The 0.5 µg/ml of Ag₂S QDs were incubated in human serum at 37 °C and the PL intensity of the QDs were measured immediately and at 48 and 72 h after incubation.

Cell Hemolysis

Hemolysis Assay in the Absence of Plasma Protein

The hemolysis assay was carried out according to ISO 10993-4:2002 [29]. Rat or healthy human blood (300 µl) was immediately mixed with 15 ml of normal physiological saline and centrifuged at 3000 rpm for 15 min. The supernatant was removed and the erythrocytes plates were washed with normal saline until the supernatant was clear. Erythrocytes were dispersed in normal saline to form a 2 % (wt) erythrocyte suspension. For the hemolytic assay, various concentrations of Ag₂S QDs were prepared by dissolving in a suspension in normal saline; 20–100 µg/ml of Ag₂S QDs were added to 1 ml erythrocyte suspension and incubated at 37 °C thermostatic water bath for 2 h. The samples tubes were centrifuged for 10 min at 3000 rpm and the optical density (OD) of the supernatants was measured at 550 nm. Samples of deionized water and normal saline were used as positive and negative control groups, respectively. The hemolysis index of each sample was calculated as:

$$\begin{aligned} & \text{Hemolysis index (\%)} \\ &= \frac{(\text{mean absorbance of test sample} - \text{mean absorbance of negative control})}{(\text{mean absorbance of positive control} - \text{mean absorbance of negative control})} \\ & \times 100 \end{aligned} \quad (4)$$

In accordance with ISO 10993-4:2002, the test sample was considered hemolytic if the hemolysis index was greater than 5 % [29]. For comparison of hemolysis activity, this method was repeated for AgNO₃.

Hemolysis Assay in the Presence of Plasma Proteins

To investigate the effect of plasma protein on cell hemolysis, hemolysis testing was repeated in the presence of 20 % plasma and protein corona. For preparation of the protein corona, the plasma was centrifuged at 3000 rpm for 15 min. Ag₂S QDs (20–100 µg/ml) were then incubated with the supernatant of centrifuged plasma) 70 % (for 2 h at 37 °C. The samples were then centrifuged at 3000 rpm for 10 min and the protein-coated QDs were washed three times with normal saline solution to remove the excess unbound plasma protein. The hemolysis assay was then repeated using corona QDs.

Cell Toxicity

Cell Culture

Human cell lines A549 (lung carcinoma) and Hep G2 (hepatocellular carcinoma) were obtained from Pasteur Institute Cell Bank of Iran (Tehran, Iran) and cultured in RPMI-1640 medium supplemented with 10 % fetal bovine serum (FBS) and 1 % penicillin streptomycin solution. The cells were incubated at 37 °C in a humidified atmosphere containing 5 % CO₂.

MTT Assay

The cytotoxicity of Ag₂S Qds for the A549 and Hep G2 human cell lines was evaluated by 3-(4,5-dimethyl-thiazol-2-yl)-2,5-diphenyltetrazolium bromide (MTT) assay. For this purpose, 1×10^4 cells were seeded in each well of 96-well culture plates and incubated for 24 h at 37 °C in a 5 % CO₂ atmosphere. Next, the cells were treated with different concentrations (6.25–200 µg/ml) of Ag₂S Qds and further incubated for 24 h and 48 h. Each well was washed three times with PBS (pH 7.0), then replaced with 100 µl of culture medium and 20 µl MTT solution (5.0 µg/ml) and incubated for another 4 h at 37 °C and 5 % CO₂ atmosphere. After removal of the MTT solution, 150 µl DMSO was added to each well and the absorbance of MTT was recorded at 490 nm using an automatic ELISA analyzer. Cell viability was calculated by following equation as:

Cell viability

$$= \frac{(\text{Mean absorbance of test wells} - \text{Mean absorbance of control wells})}{(\text{Mean absorbance of untreated wells} - \text{Mean absorbance of control wells})} \times 100 \quad (5)$$

In Vivo Imaging

A NMRI mouse weighting 30 g was shaved carefully and then anesthetized with ketamine:xylazine (80–120:10–16 mg/kg IP). Afterwards, 2 mg/kg of Ag₂S Qds was injected into the peritoneal cavity of a mouse and it was imaged using an in vivo F Pro imaging system (Bruker; USA) under excitation at 535 nm and collection at 750 nm. To confirm the Qd signal, the mouse was imaged before injection of Ag₂S Qds as a control. Animal experiments were approved by the ethics committee for animal experiments at the Shahid Beheshti Medical University, Tehran, Iran.

Statistical Analysis

The results were expressed as the mean \pm standard deviation and were analyzed by one-way ANOVA with Tukey post hoc test using SPSS 17.0 software.

Results and Discussion

Characterization of Ag₂S QDs

Hydrophilic Ag₂S QDs were prepared using a simple one-step method at 100 °C. Figure 1a shows a TEM image of the prepared particles. As demonstrated, the particles were spherical in shape and their size was <5 nm. Figure 1b shows the FT-IR spectrum of the Ag₂S QDs. The strong bands at 1283 and 1705 cm⁻¹ are typical of asymmetric and symmetric stretching modes of the carboxylate group, respectively. The peaks at 2898 and 2922 cm⁻¹ correspond to asymmetric and symmetric C–H stretching of mercaptoacetic acid, respectively. The lack of an obvious absorption peak at 2490–2560 cm⁻¹ corresponding to a free SH group [36] was noted in the FT-IR spectrum. It was concluded that the mercaptoacetic acid molecules were bound to the surface of the Ag₂S QDs by an Ag–S bond and their surfaces were carboxylic acid-terminated. The crystal structure of the Ag₂S QDs was investigated by XRD and the results are shown in Fig. 1c. The nano size of the particles produced a broad amorphous spectrum similar to those reported by Hocaoglu et al. [36]. The absorption spectrum of the Ag₂S QDs is shown in Fig. 1d.

Equations (2) and (3) were used to calculate the sizes of the Ag₂S QDs under different experimental conditions and the results are shown in Fig. 2.

The Ag₂S QDs were synthesized at three temperatures (room temperature, 50 and 100 °C) and at reaction times of 1–3 h. The crystal size and PL spectra of the QDs are shown in Figs. 2a and 3, respectively. Figure 2a shows that reaction time and

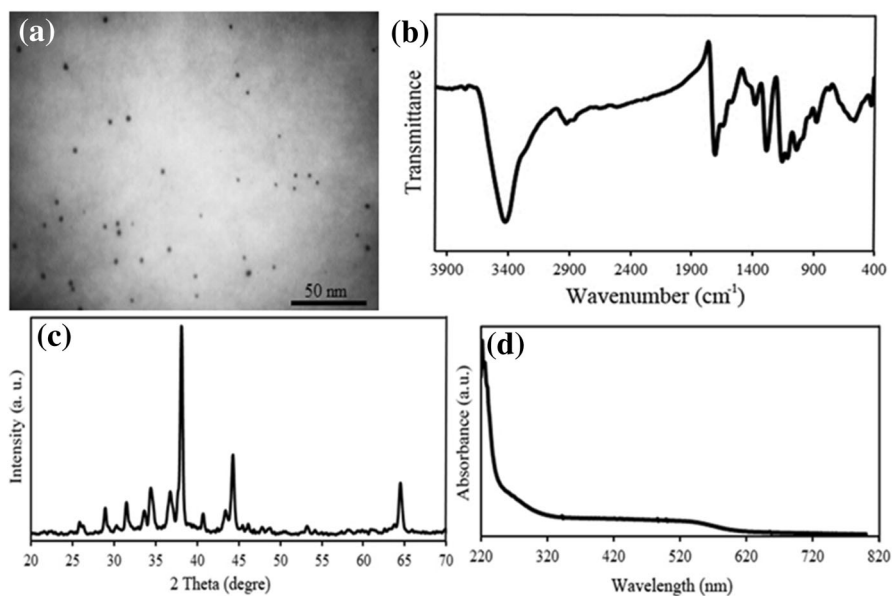


Fig. 1 a TEM image, b FT-IR spectra, c XRD pattern and d UV-Visible absorption of Ag₂S QDs (sample no. 13)

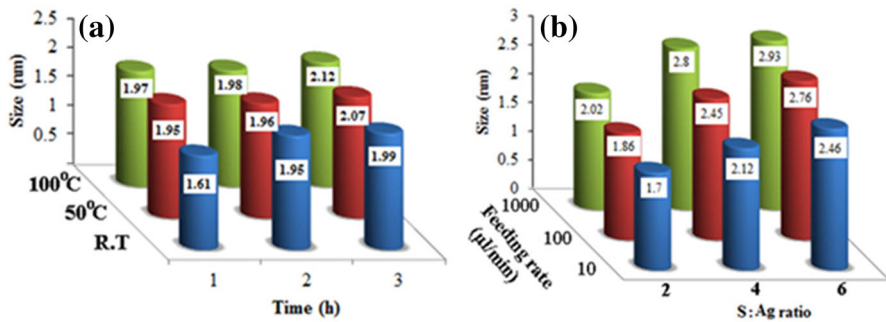


Fig. 2 Effect of: **a** time and temperature of reaction; and **b** Ag:S ratio and feeding rate on Ag₂S Qd size

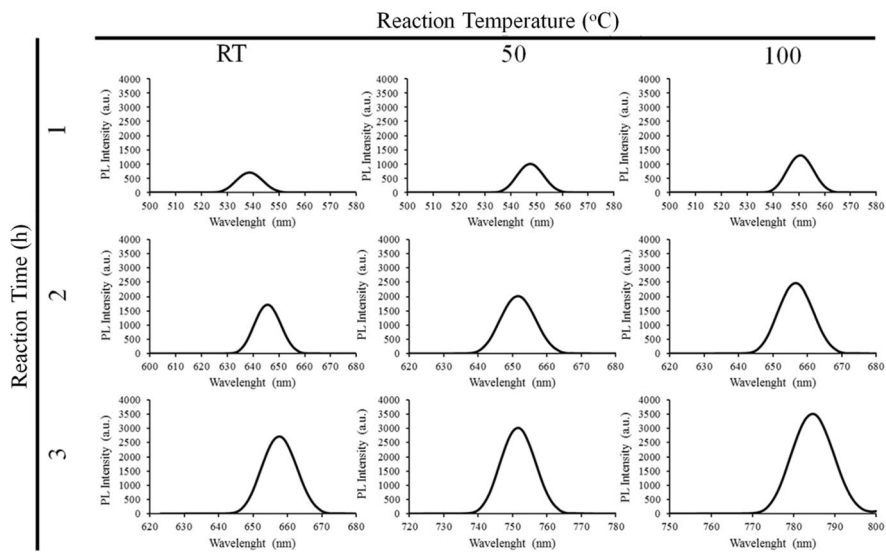


Fig. 3 PL spectra of Ag₂S Qds prepared at different reaction times and temperatures (MAA:Ag = 4; FR = 10)

temperature significantly affected Qd growth and, hence, their fluorescence. Increasing the temperature or time of the reaction caused a red shift in the absorption onset (λ_{\max} or λ_{em}), indicating an increase in Qd size with an increase in temperature or reaction time (samples 1–9; Table 1). Due to the quantum confinement effect, the smaller particles have a bigger band gap than larger particles and therefore smaller absorption wavelength.

The effect of the MAA:Ag molar ratio and the feeding rate of MAA on the particle size and PL spectra of the synthesized Qds were investigated and results are shown in Figs. 2b, 4, respectively. An increase in the MAA:Ag molar ratio (from 2 to 6) and feeding rate (10–1000 µl/min) increased the rate of crystal growth and, consequently, the size of the particles and caused a red shift in the PL spectra. Interestingly, the largest particles showed a substantial increase in PL intensity.

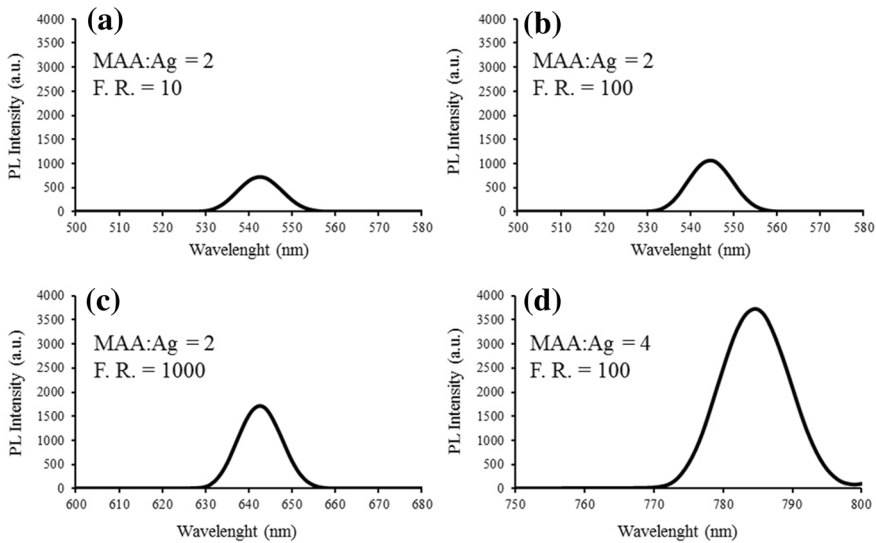


Fig. 4 PL spectra of Ag₂S QDs prepared at different MAA:Ag molar ratios and feeding rates: **a** sample 10; **b** sample 11; **c** sample 12; **d** sample 13

Figure 4d depicts the NIR-PL spectra of the Ag₂S QDs excited by a 380 nm laser diode. The emission peak centered at 785 nm is full-width at half-maximum of 30 nm, indicating a narrow size distribution for the Ag₂S QDs.

The PL stability of Ag₂S QDs was investigated and results are shown in Fig. 5. Figure 5a indicates that storage temperature markedly affected the PL spectra of the QDs. QDs stored at 37 °C showed a lower PL intensity and a maximum emission peak (λ_{em}) that shifted to higher wavelengths. This could be the result of the aggregation of QDs at a higher temperature; as the size of the QDs increased, λ_{em} shifted to higher wavelengths. The PL spectra of the Ag₂S QDs in the presence of FBS are shown in Fig. 5b. The intensity of the PL spectra of the Ag₂S QDs in the presence of FBS components decreased over time. The fluorescence intensity of the serially-diluted Ag₂S QDs (0.01, 0.1, and 0.2 μ g/ml) in PBS buffer was stored at 4 °C in either transparent or opaque vials and was monitored for 2 weeks.

The samples stored in opaque vials showed more PL stability (Fig. 5c–e vs. f–h). For example, the PL intensity of the 0.01 μ g/ml sample incubated in transparent and opaque vials for 2 weeks decreased 75 and 18 %, respectively. As expected, the PL intensity of the Ag₂S QDs was found to be concentration dependent. As the Qd concentration increased from 0.01 to 0.2 μ g/ml, the PL intensity increased. Interestingly, there was no wavelength shift in the PL spectra of the samples, indicating that the QDs were stable over the 2 weeks of storage in opaque vials at 4 °C.

Evaluation of the hemolytic properties of the QDs is a common and reliable test of toxicity and evaluation of blood component interactions. The hemolytic activity of the Ag₂S QDs fort rat and human RBCs was investigated and results are shown in Fig. 6 and Table 2. Hemolysis was evaluated for AgNO₃, Ag₂S QDs, Ag₂S

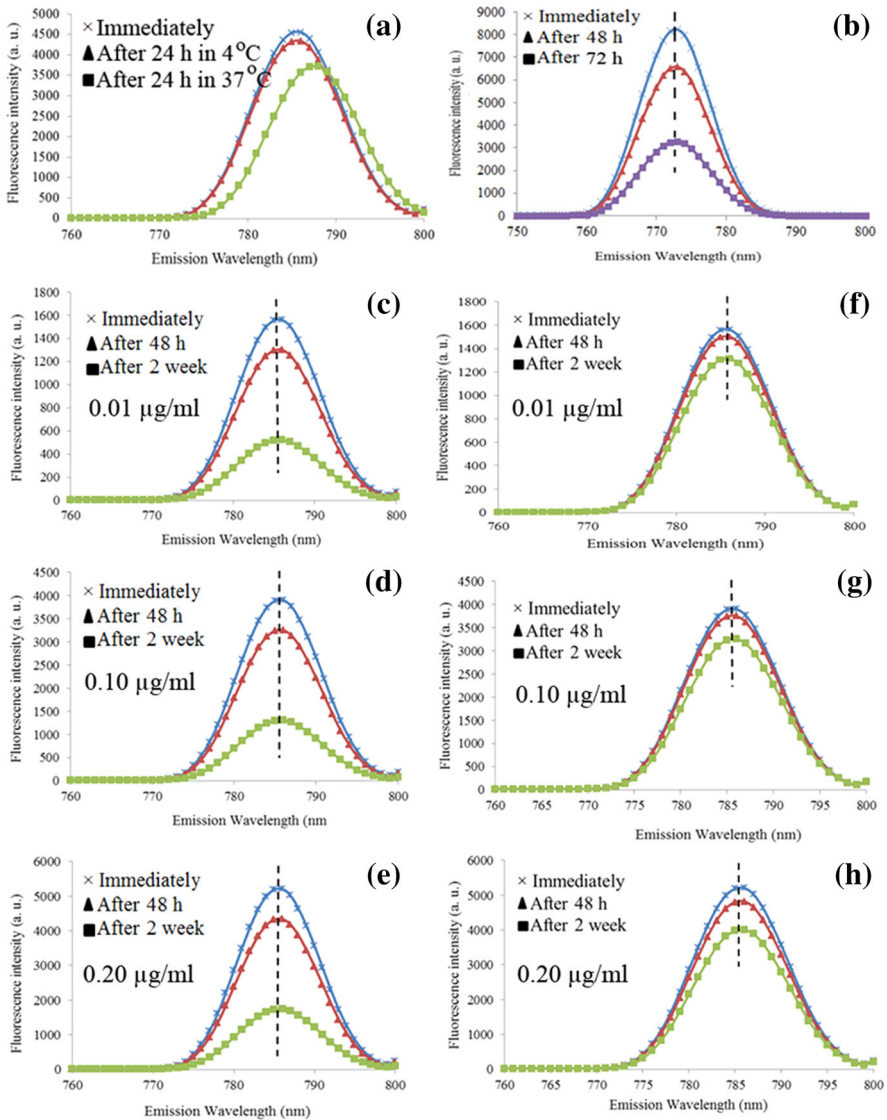


Fig. 5 Ag₂S Qds stability under different conditions. Effect of: **a** storage temperature; **b** presence of serum; **c**, **d** and **e** storage in transparent vial at 4 °C; **f**, **g** and **h** storage in opaque vial at 4 °C

Qds + 20 % plasma, and corona Qds at 20–100 μg/ml. The hemolytic activity of Ag₂S Qds differed for rat and human erythrocytes. Figure 6a shows that, for rat blood, maximum hemolysis was observed at 100 μg/ml. Figure 6b shows that, for human blood, this was observed at 40 μg/ml. Figure 6a, b indicate that Ag₂S Qds showed significantly lower hemolytic activity than AgNO₃ ($p < 0.005$).

The hemolytic activities of Ag₂S Qds were further studied in the presence of 20 % plasma protein and the results are shown in Fig. 6 and Table 2. In the

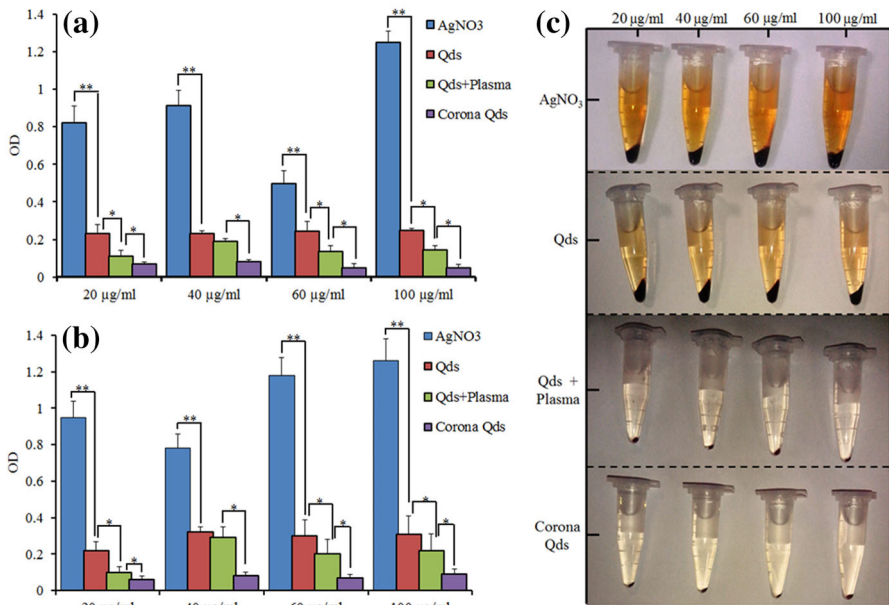


Fig. 6 Hemolysis of: **a** rat RBCs; **b** human RBCs; and **c** photograph of hemolysis of rat blood samples

Table 2 Hemolysis index of AgNO₃, Qds, Qds + Plasma and Corona Qds at different concentrations

Hemolysis index (%)	Concentration (µg/ml)			
	20	40	60	100
Rat RBCs				
AgNO ₃	17.70 ± 0.19	19.77 ± 0.13	10.41 ± 0.10	27.32 ± 0.98
Qds	4.39 ± 0.15	4.39 ± 0.16	4.73 ± 0.08	4.84 ± 0.20
Qds + plasma	1.69 ± 0.01	3.49 ± 0.03	2.27 ± 0.05	2.48 ± 0.09
Corona Qds	0.78 ± 0.01	1.01 ± 0.01	0.33 ± 0.01	0.31 ± 0.09
Human RBCs				
AgNO ₃	16.64 ± 0.91	13.47 ± 0.80	20.93 ± 0.10	22.42 ± 0.12
Qds	3.02 ± 0.05	4.88 ± 0.03	4.51 ± 0.09	4.70 ± 0.10
Qds + plasma	0.78 ± 0.03	4.32 ± 0.06	2.64 ± 0.08	3.02 ± 0.09
Corona Qds	0.03 ± 0.01	0.41 ± 0.01	0.22 ± 0.01	0.59 ± 0.01

Significant difference was observed between the hemolysis index of AgNO₃, Qds, Qds + plasma and corona Qds ($p < 0.05$)

presence of plasma protein, the degree of hemolysis was significantly lower than samples without plasma protein ($p < 0.05$). These results can be attributed to binding of proteins to the surface of the Qds and the decrease in interaction between Qds and erythrocytes. The binding of plasma proteins to surface of the Ag₂S Qds can mask and alter the chemical nature of the surface.

To further evaluate the role of plasma proteins, hemolysis was tested in the presence of protein coronas. Protein coronas were obtained by pre-incubating Ag₂S Qds with 70 % human plasma at 37 °C for 1 h [42]. The protein coronas formed within minutes after Qds exposure [43]; however, a longer incubation time was chosen to ensure protein binding. After pre-incubation, different concentrations of protein corona Qds (depending on Ag content) were added to the RBCs and results are shown in Fig. 6 and Table 2. The hemolytic activity of the protein corona Qds were significantly lower than for the other samples ($p < 0.005$).

Photographs of hemolysis test samples of rat blood erythrocytes are shown in Fig. 6c. Samples with a higher degree of hemolysis released higher amounts of hemoglobin to the supernatant. The order of hemolytic activity was: AgNO₃ > Ag₂S Qds > Ag₂S + 20 % plasma > corona Ag₂S. The upper limit of the hemolysis index is 5 %, thus, the Ag₂S Qds at the tested concentrations exhibited no hemolysis.

To investigate the toxicity induced by Ag₂S Qds, an MTT assay was conducted on A549 and Hep G2 cell lines treated 24 and 48 h at various concentrations (6.25–200 µg/mL) of Ag₂S Qds (sample 13) and results are shown in Fig. 7. The Ag₂S Qds displayed no significant toxicity for the two cell lines, even at higher doses. Furthermore, no obvious difference was observed between the 24 and 48 h results, indicating the absence of a serious toxic effect, even in the long term. Based on these results, the Ag₂S Qds could be considered as safe nanoparticles for bio-applications.

To evaluate the potential application of the Ag₂S Qds for in vivo imaging, 2 mg/kg of Qds (sample 13) were injected intraperitoneally into the mouse. The in vivo imaging results are shown in Fig. 8. Compared with the control (Fig. 8a), the injected mouse (Fig. 8b) showed bright spots of Ag₂S Qds fluorescence in the injection region. This fluorescence differed from the auto-fluorescence of the mouse body and the results suggest that the fluorescence of the Ag₂S Qds could penetrate from the body of the mouse and is appropriate for in vivo imaging.

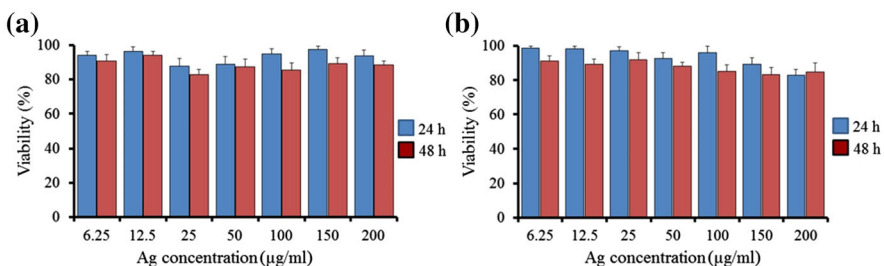


Fig. 7 Cell viability of: **a** A549; and **b** Hep G2 cell lines after 24 and 48 h of incubation at different concentrations of Ag₂S Qds. No significant difference was observed between control and Qds treated cells ($p > 0.05$)

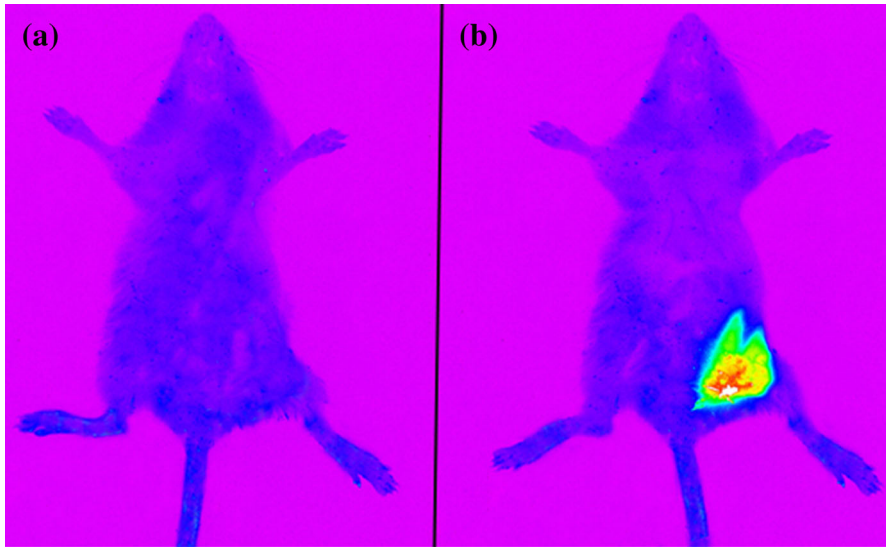


Fig. 8 In vivo imaging of mouse: **a** prior to inoculation (control); and **b** after injection of 2 mg/kg of Ag_2S Qds IP

Conclusions

Hydrophilic Ag_2S Qds were successfully prepared by the reaction of mercaptoacetic acid and AgNO_3 . The size of the Qds increased and PL spectra shifted to higher wavelengths with an increase in temperature, time, MAA:Ag molar ratio, and feeding rate. The PL spectra of the samples indicate that the Qds were stable over the 2 weeks of storage in opaque vials at 4 °C. The Ag_2S Qds showed good biocompatibility and no significant toxicity was observed for the A549 and Hep G2 cell lines. The effect of plasma and corona proteins on the hemolytic activity of the Ag_2S Qds on rat and human RBCs was investigated and no hemolysis was observed at the tested concentrations. The ability of Qds as an in vivo imaging marker was tested by intraperitoneal injection of mice. The results showed that the Ag_2S Qds penetrated the body of the mouse with excellent PL brightness. It was shown that the Qds can be applied as biocompatible NIR probes for in vivo imaging.

Acknowledgments This study was supported by a Grant from Shahid Beheshti University of Medical Sciences.

Compliance with Ethical Standards

Conflicts of Interest The authors report no conflicts of interest.

References

1. J. Jaber and E. Mohsen (2013). *Colloids Surf. B* **102**, 265.

2. S. Han, Y Mu Q Zhu, Y. Gao, Z. Li, Q. Jin, and W. Jin (2012). *Anal. Bioanal. Chem.* **403**, 1343.
3. M. Salavati-Niasari, J. Javidi, and M. Dadkhah (2013). *Comb. Chem. High Throughput Screen.* **16**, 458.
4. A. Jaganathan, K. Murugan, C. Panneerselvam, P. Madhiyazhagan, D. Dinesh, C. Vadivalagan, A. T. Aziz, B. Chandramohan, U. Suresh, R. Rajaganesh, J. Subramaniam, M. Nicoletti, A. Higuchi, A. A. Alarfaj, M. A. Munusamy, S. Kumar, and G. Benelli (2016). *Parasitol. Int.* **65**, 276.
5. K. Murugan, D. Dinesh, K. Kavithaa, M. Paulpandi, T. Ponraj, M. S. Alsali, S. Devanesan, J. Subramaniam, R. Rajaganesh, H. Wei, S. Kumar, M. Nicoletti, and G. Benelli (2016). *Parasitol. Res.* **115**, 1085.
6. G. Benelli, A. Lo Iacono, A. Canale, and H. Mehlhorn (2016). *Parasitol. Res.* **115**, 2131.
7. G. Benelli (2016). *Parasitol. Res.* **115**, 23.
8. B. Ballou, B. C. Lagerholm, L. A. Ernst, M. P. Bruchez, and A. S. Waggoner (2004). *Bioconjug. Chem.* **15**, 79.
9. W. Cai, D. W. Shin, K. Chen, O. Gheysens, Q. Cao, S. X. Wang, S. S. Gambhir, and X. Chen (2006). *Nano Lett.* **6**, 669.
10. S. R. Sershen, S. L. Westcott, N. J. Halas, and J. L. West (2000). *J. Biomed. Mater. Res.* **51**, 293.
11. E. B. Voura, J. K. Jaiswal, H. Mattoussi, and S. M. Simon (2004). *Nat. Med.* **10**, 993.
12. F. Erogbogbo, K. T. Yong, I. Roy, G. X. Xu, P. N. Prasad, and M. T. Swihart (2008). *ACS Nano* **2**, 873.
13. K. Welsher, Z. Liu, S. P. Sherlock, J. T. Robinson, Z. Chen, D. Daranciang, and H. Dai (2009). *Nat. Nanotechnol.* **4**, 773.
14. K. Welsher, S. P. Sherlock, and H. Dai (2011). *Proc. Natl. Acad. Sci. USA* **108**, 8943.
15. G. X. Liang, M. M. Gu, J. R. Zhang, and J. J. Zhu (2009). *Nanotechnology* **20**, 415103.
16. H. Chen, S. Cui, Z Tu J Ji, J. Zhang, and Y. Gu (2011). *Photochem. Photobiol.* **87**, 72.
17. B. Blackman, D. Battaglia, and X. Peng (2008). *Chem. Mater.* **20**, 4847.
18. R. G. Aswathy, Y. Yoshida, T. Maekawa, and D. S. Kumar (2010). *Anal. Bioanal. Chem.* **397**, 1417.
19. C. Li, F. Li, Y. Zhang, W. Zhang, X. E. Zhang, and Q. Wang (2015). *ACS Nano* **9**, 12255.
20. Y. Zhang, G. Hong, Y. Zhang, G. Chen, F. Li, H. Dai, and Q. Wang (2012). *ACS Nano* **6**, 3695.
21. C. N. Zhu, P. Jiang, Z. L. Zhang, D. L. Zhu, Z. Q. Tian, and D. W. Pang (2013). *ACS Appl. Mater. Interfaces* **5**, 1186.
22. G. Hong, J. T. Robinson, Y. Zhang, S. Diao, A. L. Antaris, Q. Wang, and H. Dai (2012). *Angew. Chem. Int. Ed.* **51**, 9818.
23. P. Jiang, C. N. Zhu, Z. L. Zhang, Z. Q. Tian, and D. W. Pang (2012). *Biomaterials* **33**, 5130.
24. L. Tan, A. Wan, and H. Li (2013). *ACS Appl. Mater. Interfaces* **5**, 11163.
25. L. Tan, A. Wan, and H. Li (2013). *Langmuir* **29**, 15032.
26. H. Chen, B. Li, M. Zhang, K. Sun, Y. Wang, K. Peng, M. Ao, Y. Guo, and Y. Gu (2014). *Nanoscale* **6**, 12580.
27. Y. Wang and X. P. Yan (2013). *Chem. Commun.* **49**, 3324.
28. Y. Du, B. Xu, T. Fu, M. Cai, F. Li, Y. Zhang, and Q. Wang (2010). *J. Am. Chem. Soc.* **132**, 1470.
29. H. Y. Yang, Y. W. Zhao, Z. Y. Zhang, H. M. Xiong, and S. N. Yu (2013). *Nanotechnology* **24**.
30. S. K. Maji, S. Sreejith, A. K. Mandal, A. K. Dutta, and Y. Zhao (2014). *Anal. Methods* **6**, 2059.
31. J. Liu, P. Raveendran, Z. Shervani, and Y. Ikushima (2004). *Chem. Commun.* **10**, 2582.
32. X. Chen, L. Ding, P. Liu, and Q. Wang (2014). *Surf. Interface Anal.* **46**, 301.
33. Y. Zhang, Y. Liu, C. Li, X. Chen, and Q. Wang (2014). *J. Phys. Chem. C* **118**, 4918.
34. P. Jiang, Z.-Q. Tian, C.-N. Zhu, Z.-L. Zhang, and D.-W. Pang (2012). *Chem. Mater.* **24**, 3.
35. G. A. Martínez-Castañón, M. G. Sánchez-Loredo, H. J. Dorantes, J. R. Martínez-Mendoza, G. Ortega-Zarzosa, and F. Ruiz (2005). *Mater Lett* **59**, 529.
36. I. Hocaoglu, M. N. Cizmeciyan, R. Erdem, C. Ozen, A. Kurt, A. Sennaroglu, and H. Y. Acar (2012). *J. Mater. Chem.* **22**, 14674.
37. M. Lundqvist, J. Stigler, G. Elia, I. Lynch, T. Cedervall, and K. A. Dawson (2008). *Proc. Natl. Acad. Sci. USA* **105**, 14265.
38. A. Ergene, S. Tan, H. Katircioğlu, and Z. Oktem (2006). *Fresenius Environ. Bull.* **15**, 283.
39. C. Jaafar-Maalej, R. Diab, V. Andrieu, A. Elaissari, and H. Fessi (2010). *J. Liposome Res.* **20**, 228.
40. L. E. Brus (1984). *J. Chem. Phys.* **80**, 4403.
41. S. H. Ehrlich (1993). *J. Imaging Sci. Technol.* **37**, 73.
42. J. Shi, Y. Hedberg, M. Lundin, I. Odnevall Wallinder, H. L. Karlsson, and L. Möller (2012). *Acta Biomater.* **8**, 3478.
43. A. J. Paula, D. S. T. Martinez, R. T. A. Júnior, A. G. S. Filho, and O. L. Alves (2012). *J. Braz. Chem. Soc.* **23**, 1807.